Chapter

2

Materials, methods, and characterization techniques

Contents

In this chapter, the methods used for the synthesis and functionalization of GO/metal oxide NCs have been described. Also, various experimental techniques have been used for the characterization of NCs. Additionally, this chapter includes a description of the different experimental setups used in this study.

2.1 Introduction

Recent development in the technologies is rely on materials. Synthesis and characterization of materials is the first and foremost important steps in the experimental research. Number of novel methods have been established for the preparation of good quality materials. Moreover, proper selection of synthesis method helps to carry out desired properties in the samples to be characterized along with desired potentials.

In the early part of the present chapter, the list of sources of material used in the synthesis is stated followed by experimental technique used for the synthesis of material and various characterization techniques are thoroughly detailed and discussed in detail.

2.2. Materials

Graphene oxide (GO), cationic gemini surfactant (CGS), and deep eutectic solvent (DESs) are synthesized and characterized using the same procedures as reported previously [1–5]. Graphite fine powder (99%, AR grade), potassium permanganate ($KMnO_4$; 99%, AR grade), zirconium acetate [$Zr(CH_3COO)_2$] (99%, AR grade), Titanium isopropoxide (TTIP, $Ti[OCH(CH_3)_2]_4$), glacial acetic acid (CH_3COOH), zinc acetate [$Zn(CH_3COO)_2$], hydrogen peroxide 30% solution (H_2O_2; AR grade), methylene blue (MB), congo red (CR) and rhodamine B (RB) microscopic grade (98%), sodium dodecyl sulfate (SDS, 99%, AR grade), cetyltrimethylammonium bromide (CTAB, 99%, AR grade), dodecyl trimethyl ammonium bromide (DTAB, 99%, AR grade), choline chloride (ChCl, 99%, AR grade), urea (99%, AR grade), Glycerol (98%, AR grade), dichloromethane (DCM, 99%, AR grade), acetone (99%, AR grade) and methanol (99%, AR grade) have been purchased from Sigma Aldrich (India). Absolute alcohol (99.5%) was provided by Applied Chemistry Department, The Maharaja Sayajirao University of Baroda, India (Gujarat government approved). Absolute ethanol was dried by using of magnesium /iodine and stored on molecular sieves. Polycarbonate (PC) and polystyrene (PS) polymers have been obtained from Fluoro Polymer Industries Pvt. Ltd (India). The distilled water of specific conductance ~1 $\mu S\ cm^{-1}$ was used throughout. All the other chemicals used are of AR grade and used as received. Structures of all the materials used in the study are depicted in **Scheme 2.1**.

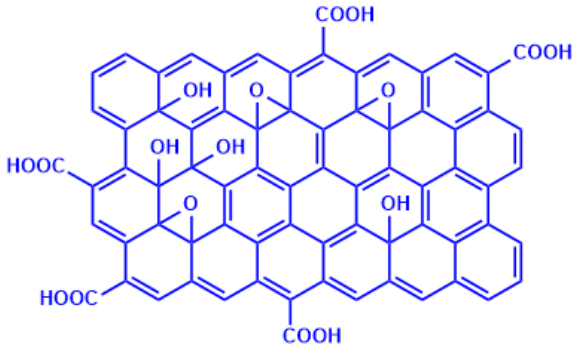

Graphene Oxide

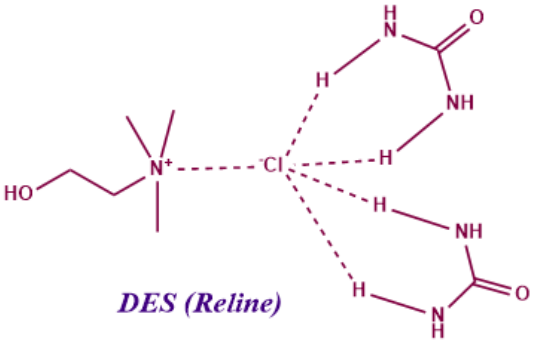

DES (Reline)

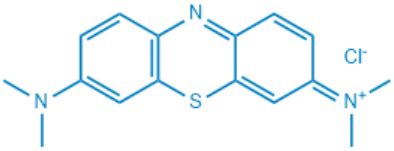

Methylene blue (MB)

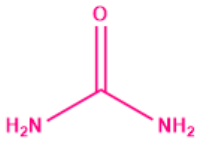

Urea

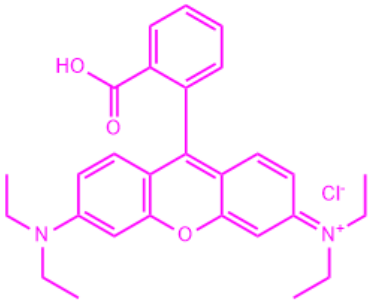

Rhodamine B (RB)

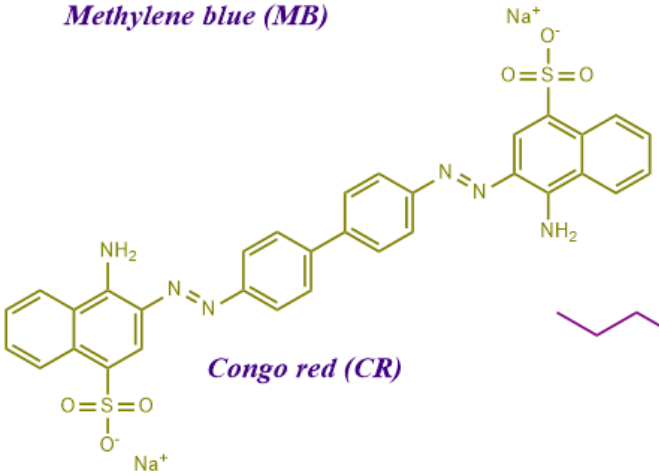

Congo red (CR)

Cetyltrimethylammonium bromide (CTAB)

Dodecyltrimethylammonium bromide (DTAB)

sodium dodecyl sulphate (SDS)

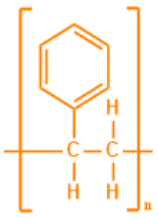

Polystyrene (PS)

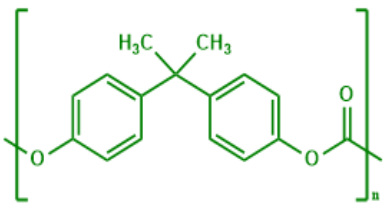

Polycarbonate (PC)

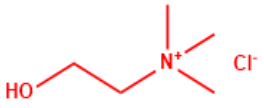

Choline chloride (ChCl)

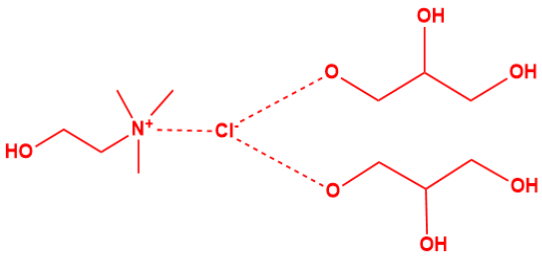

Glyceline

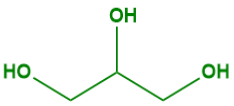

Glycerol

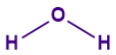

Water

Scheme 2.1: Chemical structures of material used.

2.3 Methods

2.3.1. Synthesis of graphene oxide

Graphite flakes, more economically and abundantly accessible in nature, served as the precursor for the preparation of GO using a modified Hummers' method [6–8]. This approach involves the oxidation and exfoliation of graphite sheets, incorporating both sonication and thermal treatment. The sequential synthesis of GO is summarized briefly as follows:

Graphite powder was suspended in a mixture of H_2SO_4, HNO_3, and H_3PO_4 (in a ratio of 7:2:1) with continuous stirring. A slow addition of $KMnO_4$ was maintained out by keeping the suspension in an ice bath. The ice bath was replaced with a water bath and the suspension was stirred again for 2 h at 40°C. 200 mL of water was gradually added to the suspension (below 90°C). 20 mL of 30% aqueous H_2O_2 was added (under stirring) to the suspension which resulted in a colour change from brown to greenish-yellow that shows the formation of GO. The GO was washed twice with 1:10 HCl solution followed by water till neutrality. The decanted product was dispersed in the water again and subjected to sonication for 30 m (to achieve exfoliation of GO). The resulting suspension was centrifuged at 700 rpm for 20 m to remove any remaining exfoliated graphite. Finally, the obtained thick mass of GO was dried in a vacuum oven for 24 h at 55°C. Step by step procedure is shown in **Scheme 2.2**.

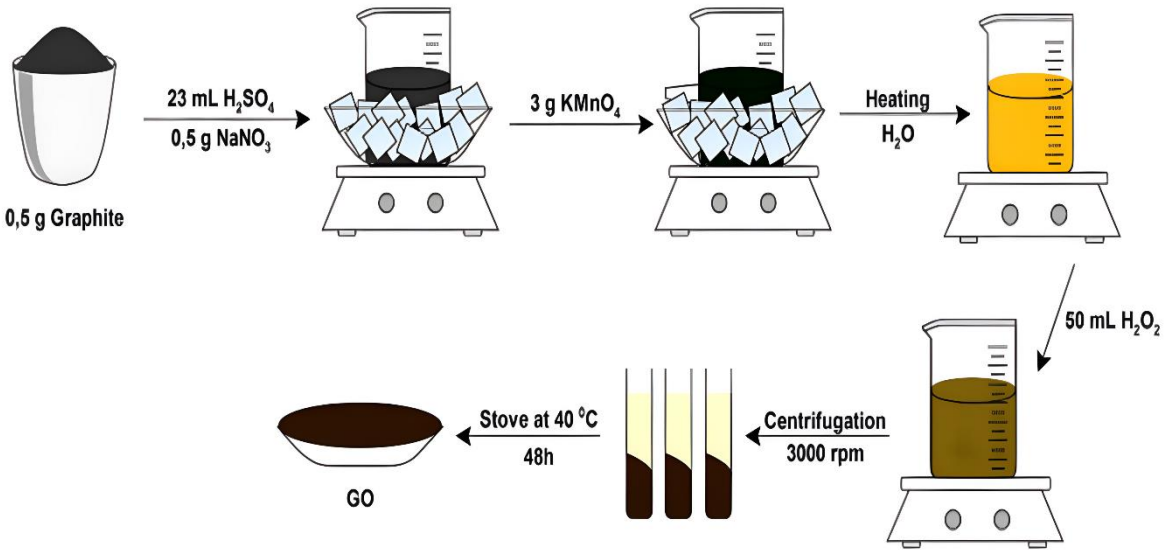

Scheme 2.2: Synthesis of graphene oxide

2.3.2 Synthesis of GO@ZrO_2 nanocomposite

Synthesis of GO@ZrO_2 nanocomposite (NC) involved the following steps (**Scheme 2.3**) [9–11]: Initially, GO was dispersed in an aqueous solution (1 g in 100 ml) through sonication for 30 m. The resulting dispersion was then stirred with an aqueous solution of zirconium acetate (1 g in 100 ml) for 30 m. Subsequently, the mixture underwent another round of sonication for 1 h, followed by the gradual addition of 20 ml of 1M NaOH. The resulting mixture was heated to 100°C while being continuously stirred (2 h). A color change from greenish yellow to black indicated the formation of the dispersed aqueous GO@ZrO_2 NC. The black dispersed solution was filtered, and the solid mass was washed with ethanol and then distilled water (50 ml every 3 times). Finally, the GO@ZrO_2 NC was obtained as a black powder after drying at 100°C for 12 h in a vacuum oven.

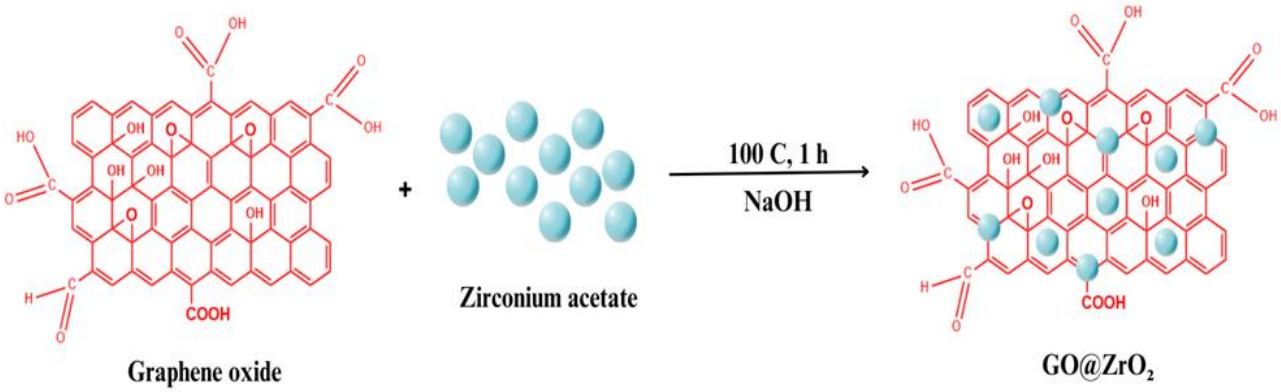

Scheme 2.3: Synthesis of GO@ZrO_2 NC

2.3.3 Synthesis of GO@TiO_2 nanocomposite

TiO_2 nanoparticles (NPs) were synthesized by the sol-gel method [12]. In brief, a homogenous solution consisting of 17 mL of TTIP and 50 mL of ethanol was incrementally delivered in the form of droplets to a mixture composed of 30 mL of ethanol, 10 mL of glacial acetic acid, and 10 mL of distilled water. The mixture was continuously stirred for an additional hour. Following a 24 h aging process in a 70°C water bath, the resulting sol was subjected to drying in a vacuum oven at 90°C for 12 h, followed by calcination for 2 h at 500°C to obtain the TiO_2 NPs.

The synthesis procedure for GO@TiO_2 NC begins with the dispersion of GO in a 100 mL aqueous solution (1 g) using 30 m of sonication [13,14]. Following this, the resulting dispersion is combined with an aqueous solution of TiO_2 NPs (1 g in 100 mL), and stirring is conducted at 100°C for a duration of 2 h. Subsequently, the mixture undergoes filtration, and the solid mass is subjected to three washes with distilled water, followed by ethanol (50 mL each). The resultant material, GO@TiO_2 NC, is then dried at 100°C for 12 h in a vacuum oven, resulting in the production of a black powder.

2.3.4 Synthesis of GO@ZnO nanocomposite

The synthesis of ZnO NPs involves the following steps: 2 g of zinc acetate dihydrate [$Zn(CH_3COO)_2$] were first dissolved in 20 mL of deionized water [15,16]. This aqueous solution of $Zn(CH_3COO)_2$ was then heated to 70 ºC with continuous stirring using a magnetic stirrer. Subsequently, a freshly prepared NaOH (4 g) solution was added dropwise into $Zn(CH_3COO)_2$ solution under constant stirring, and the mixture was refluxed for 4 h at 70 ºC. After filtering and properly washing with deionized water, the resultant white suspension was (maintaining the pH up to 6), dried in an air oven at 70°C, and finally calcined at 550°C for 6 h to obtain a white powder of ZnO NPs.

The synthesis of GO@ZnO NC includes the following steps: GO was dispersed in an aqueous solution (1 g in 100 ml) through 30 m of sonication. The resulted dispersion was mixed with aqueous ZnO NPs (1 g in 100 ml) and stirring was conducted at 100°C for 2 h. Subsequently, the mixture was filtered, and the solid mass was subjected to three washes with distilled water and then with ethanol (50 ml each). The material, GO@ZnO NC, was dried for 12 h in a vacuum oven at 100°C, yielding a black powder.

2.3.5 Functionalization of nanocomposites with surfactants

The synthesized NCs (GO@ZrO_2, GO@TiO_2 and GO@ZnO) was modified with the surfactant using the following procedure (**Scheme 2.4**) [3,10,17]. NCs (3 g/100 mL) has been stirred in aqueous surfactant (DTAB/CTAB/CGS) solution (0.5 g/100 ml). The resulting mixture was subjected to 5 m of sonication and then gently stirred at room temperature for an additional 2 h. The obtained dispersion was subsequently subjected to centrifugation at 3000 rpm for 10 m and underwent three consecutive washes, with each wash involving 50 ml of distilled water. This gives surfactant-modified NCs after drying for 12 h at 65°C in a vacuum oven.

2.3.6 Preparation of DESs

2.3.6.1 Preparation of reline

Reline was synthesized and characterized using the same procedure as previously reported [5]. Briefly, dried ChCl and urea (1:2 molar ratio) were mixed and heated at 80°C for approximately 2 h with continuous stirring till the appearance of clear fluid. This fluid was equilibrated for 24 h (in a vacuum oven) at 40°C.

2.3.6.2 Preparation of glyceline

Glyceline was synthesized and characterized using the same procedure as previously reported [18]. Briefly, dried ChCl and glycerol (1:2 molar ratio) were mixed and heated at 80°C for approximately 2 h with continuous stirring till the appearance of clear fluid. This fluid was equilibrated for 24 h (in a vacuum oven) at 40°C.

2.3.6.3 Preparation of aquoline

Aquoline was formed by following a reported procedure [19] in which dried choline chloride and water (κ~2.0 $\mu S.cm^{-1}$) were mixed in different compositions (1:2, 1:3, 1:4 and 1:5) followed by stirring for 30 m under ambient conditions. Transparent homogenous fluid so obtained were equilibrated for 1 h in a paraffin sealed bottle and later on stored in a desiccator.

2.3.7 Functionalization of nanocomposites with DES

1 g of NCs (GO@ZrO_2, GO@TiO_2 and GO@ZnO) was sonicated with 10 mL of DES for 30 m to get homogeneous dispersion [10]. After being transferred to a round-bottom flask, this dispersion was stirred for 2 h at 80°C. The mixture was filtered and washed several times with distilled water followed by ethanol. This DES-modified NCs was dried in a vacuum oven at 80°C for 24 h (**Scheme 2.4**).

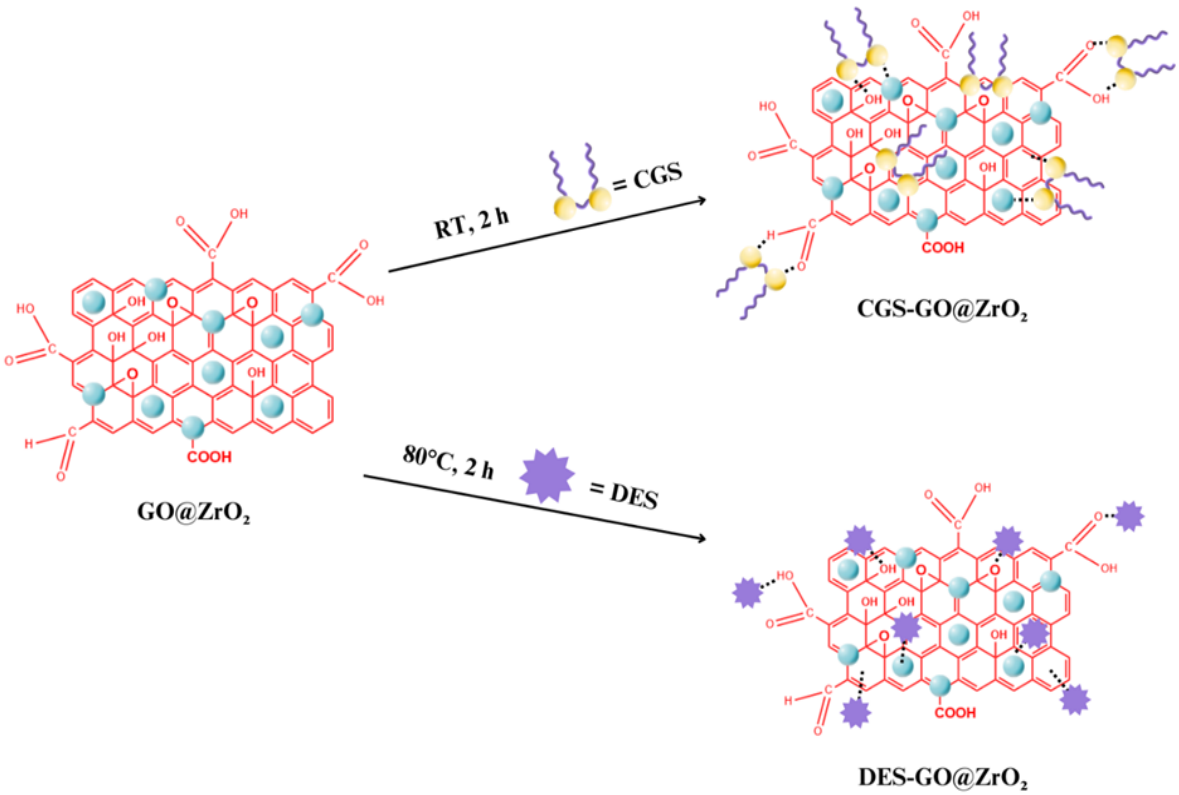

Scheme 2.4: Synthesis of surfactant/DES modified NCs

2.3.8 Fabrication of mixed matrix membranes from PC/PS blend and nanofillers

Scheme 2.5 shows the preparation of mixed matrix membranes **(**MMMs) using different nanofillers. PC and PS polymers were dissolved in DCM (process of solution casting). A blend of polymeric films of PC/PS was prepared using the phase inversion method [20]. To get a homogenous solution, the solution of PC and PS blend was individually stirred for 3 h in 12 mL DCM at 300 rpm. This mixture of PC/PS (50/50 weight ratio, w/w%) with different weight percentages (wt%) of nanofillers (GO, ZrO_2, GO/ZrO_2, DES-GO/ZrO_2 (with 2 wt%, 5 wt%, 7 wt%, 10 wt%, 15 wt% and 20 wt%)) were sonicated for 1 h by using an ultra-sonicator. The whole mixture was stirred again for 24 h at ambient temperature. The solution was drained on a flat glass plate, swapped by a 100 μm thickness rod and the solvent was left to evaporate. The dried films (MMMs), after being taken out of the glass plate, were tested for permeability. (MMMs), after being taken out of the glass plate, were tested for permeability. MMMs uniform thickness was verified using a digital thickness meter (which varied from 84-88 μm).

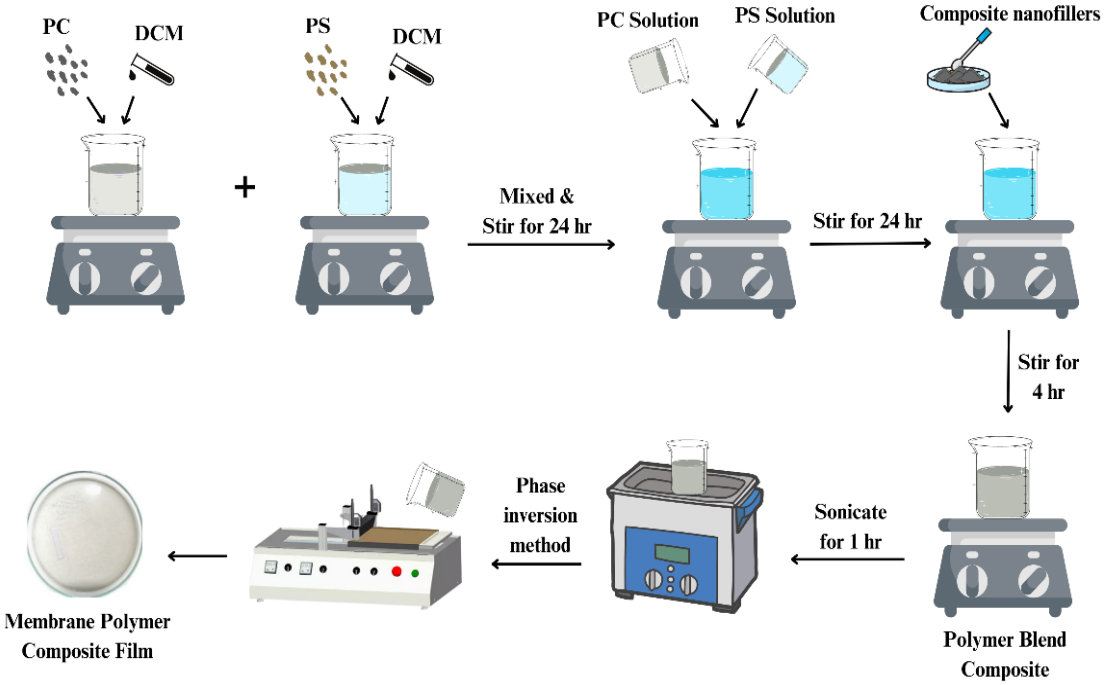

Scheme 2.5: Preparation of MMMs film with different nanofillers using the phase inversion method.

2.3.9 Dye adsorption study

Adsorption data were obtained through batch experiments, conducted in triplicate. The concentration of dye was determined using an external calibration method with a peak wavelength at λ_{max} (MB=663nm), resulting in a good correlation line (not displayed) with R^2~0.999, which was utilized for quantifying dye adsorption. In these experiments, a 20 ml solution of the dye with various concentrations was mixed with various composite dosages in quick-fit glass bottles. The mixtures were allowed to equilibrate under ambient conditions for different time intervals depending on the specific nature of the study, whether it involved adsorption or kinetics [21,22]. After the specified equilibration period, the mixtures were centrifuged, and UV-vis investigations were carried out using a UV-1800 instrument from Shimadzu, Japan. The composite adsorption capacity (Q) was calculated using the following expression,

$$Q = \frac{(C_i - C_t)}{C_i} \times \frac{V}{w} \quad (1)$$

where C_i and C_t represent the initial and time t concentrations of dye, respectively. V stands for the volume of the dye solution, and w represents the weight of the modified composite (adsorbent). Furthermore, the percentage of dye removal (P) was calculated using the following mathematical expression,

$$P = \frac{(C_i - C_t)}{C_i} \times 100 \quad (2)$$

2.3.10 Determination of pH at the point of zero charge (pH_{pzc})

The point of zero charge (pH_{pzc}) of NCs was determined using the salt addition method [23]. This involved the use of a 0.1 M KNO_3 solution at 30°C. The total volume of the solution was precisely adjusted to 20 mL in a conical flask by adding 0.1 M KNO_3. The initial pH ($pH_{initial}$) of the solutions was regulated within the range of 2.0 to 12.0 by introducing 0.1 M HCl and 0.1 M NaOH solutions as necessary. These solutions with different $pH_{initial}$ values were then mixed with 50 mg of the NC, and the suspensions were allowed to stand for 24 h. The final pH (pH_{final}) of the supernatant liquid was recorded for each solution. The difference between the $pH_{initial}$ and pH_{final} ($\Delta pH = pH_{initial} - pH_{final}$) was then plotted against $pH_{initial}$. The point of intersection of the resulting curve with the abscissa, where $\Delta pH=0$, gives the pH_{pzc}.

2.3.11 Dye re-adsorption study

The adsorbed dye was removed from the adsorbent by washing it three times with 50 ml of ethanol on each occasion. After each washing, the adsorbent was filtered, and the washed adsorbent was subsequently dried in a vacuum oven for 12 h at 80°C. The recharged NCs obtained in this manner were utilized for the re-adsorption of dye for up to the few cycles. The re-adsorption efficacy (R_e) was calculated using the following expression,

$$R_e = \frac{Q_r}{Q_f} \times 100 \quad (3)$$

where Q_r and Q_f are adsorption capacities with recharged and fresh NCs.

2.3.12 Gas permeability measurements

A bubble flow meter has been used in the constant pressure/variable volume system to measure the rate of flow of gas molecules which is shown in **Figure 2.1.** The feed gas supplied by the gas cylinder is allowed to flow via the valve that joins it to the feed side of the gas permeability cell [24–26]. Now that the target gas has been injected at 30 psi constant pressure towards the membrane's upstream face, the bubble flow meter has been used to measure the steady state gas flux from the downstream side of the membrane. The bubble flow meter would display the rate of volume change over time for each distinct bubble on the screen if we could only reach one bubble at the top of the capillary tube, permitting us to monitor only one bubble.

The gas molecules move through the membrane of the bubble flow meter to the downstream side flows. The experiment has been performed several times to get an accurate

measurement. The following Eq. (4) has been used to determine the permeability of the system in a steady state:

$$\boldsymbol{P} = \frac{l}{P_1 - P_2} \times \frac{P_{atm}}{ART} \times \frac{dv}{dt} \qquad (4)$$

The pressure difference between the membrane's upstream and downstream sides is (P_2-P_1), P_1 is sufficiently small compared to P_2, so we can only consider P_2 in the calculation. Where dv/dt is the rate of change in gas flow that penetrates the membrane, A is the membrane's area in cm^2, P_{atm} is atmospheric pressure (1 atm = 76 Hg.cm), and l is the membrane's thickness in cm. The temperature T is measured in degrees Celsius (°C), whereas the universal gas constant R is expressed in $cmHg.cm^3/(STP)\ cm^3°K$. This system determined the unit Barrer's for gas permeability measurement.

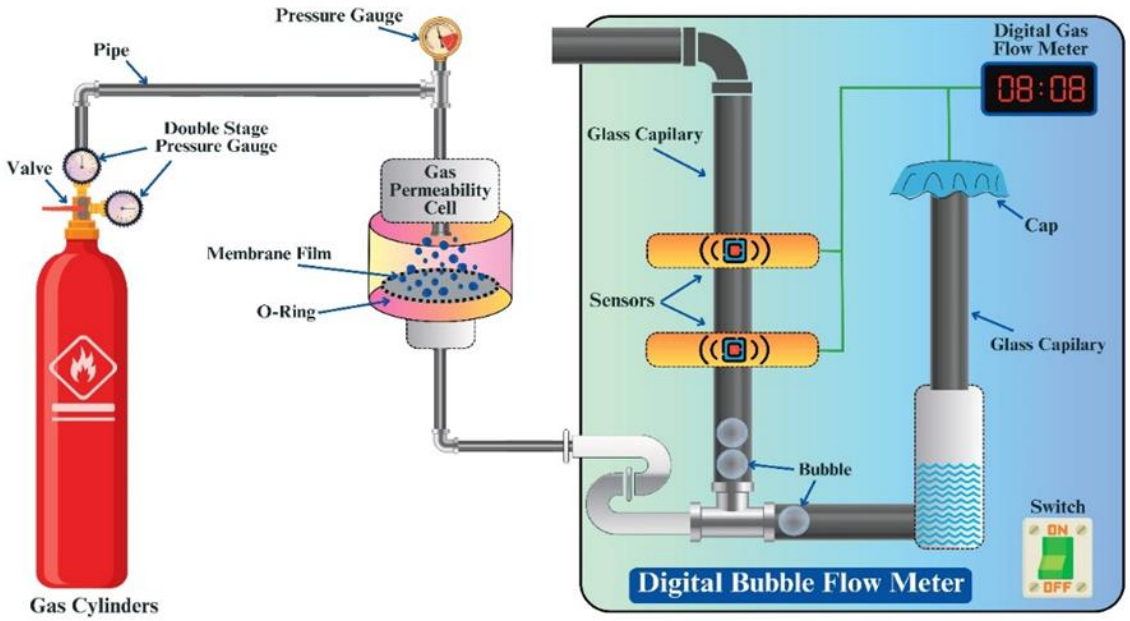

Figure 2.1: Schematic diagram of bubble flow meter-based system with constant pressure/variable volume.

2.3.13 Porosity by dry-wet weight technique

The membrane's porosity was evaluated using the dry-wet weight technique [27,28]. Samples of the membrane measuring 4 cm by 4 cm were cut and placed in water overnight. The weight was measured while they were submerged using an analytical balance. Subsequently, the membrane was taken out, and any surface water was carefully removed with filter paper after soaking in distilled water at ambient temperature for 24 h. These membrane samples were then allowed to air dry at ambient temperature overnight, and after their dry weight was determined.

All weight measurements were consistently recorded on an analytical balance, and a digital thickness meter was employed to measure the sample's thickness on both sides twice. Using the information and the subsequent Eq. (5), the porosity has calculated:

$$\boldsymbol{\alpha} = \frac{W_{Wet} - W_{dry}}{a.\ t.\ \rho} \quad (5)$$

Where α = Membrane Porosity (%), Weights are expressed as W_{wet} (g) for the wet membrane and W_{dry} (g) for the dry membrane (g), a= Membrane films effective surface area (cm^2), t = Membrane films thickness, and ϱ = Water density (g/cm^3).

2.4 Characterization techniques

Various spectroscopic, thermal, and microscopic techniques were employed to characterize the materials synthesized in this research work. The structural properties were assessed through Fourier transform infrared spectroscopy (FTIR). X-ray diffraction studies (XRD) were conducted to analyze the crystallinity of the samples and calculate the interlayer distance of graphene. UV-visible absorption spectroscopy (UV-Vis) was utilized for studying the characteristic dye adsorption of the samples. The thermal decomposition patterns were investigated through thermogravimetric analysis (TGA) and differential scanning calorimetry (DSC). The morphology and surface features were examined using field emission scanning electron microscopy (FESEM) and transmission electron microscopy (TEM). Elemental composition analysis was carried out using energy dispersive X-ray (EDX). Tensile experiments were conducted to analyze the mechanical characteristics of the blend nanocomposite structures. A bubble flow meter has been used in the constant pressure/variable volume system to measure the rate of flow of gas molecules. The contact angle measurement is a technique used to understand how a liquid interacts with a solid surface.

2.4.1 Fourier transform infrared spectroscopy (FTIR)

FTIR, a popular technique for structural analysis [29], functions based on the concept that molecules display distinctive absorption peaks associated with the vibrational frequencies of bonds between atoms within the substance. Molecules exhibit specific frequencies at which they undergo rotation or vibration, corresponding to discrete energy levels. In an infrared spectrometer, the sample is exposed to infrared radiation with gradually increasing wavelengths, and the absorbance percentage is gauged. The resultant spectrum functions as the molecular signature of the sample, as various functional groups absorb at their specific characteristic frequencies.

Figure 2.2: Fourier transform infrared spectroscopy (FTIR-8400S, Shimadzu, Japan) used for the present work.

FTIR spectra were performed using an FTIR-8400S instrument manufactured by Shimadzu, Japan, covering the spectral range of 4000-400 cm^{-1} in the KBr transmission mode. Pellets were created by mixing the samples with KBr and subjecting them to a pressure of 4 tons using a hydraulic press (Techno search instruments, Mumbai). Upon exposure to radiation, specific incident frequencies corresponded with molecular vibrations. This resonance permitted the transmission of energy among the incident electromagnetic wave and molecular vibrations, with the absorbed frequencies reported as a spectrum.

2.4.2 X-ray diffraction (XRD)

X-ray diffraction (XRD) serves as an effective technique for interpreting the structural characteristics of crystalline materials [30]. In this method, X-rays are generated by a cathode-ray tube and then filtered to produce monochromatic X-rays. These monochromatic X-rays are subsequently collimated to focus and direct them towards the sample. As the X-rays pass through the crystal, they create a diffraction pattern due to their wavelength matching the atomic bond length. The resulting patterns provide insights into the crystal structure. The scattered X-rays may undergo either constructive/destructive interference, a phenomenon explained by Bragg's Law [31].

$$n\lambda = 2d\sin\theta \quad (6)$$

Figure 2.3: X-ray diffractometer (SmartLab, Rigaku Corporation, Japan) used for the present work

The atoms in the crystal lattice determine the diffracted wave's intensities, and the dimensions and form of the material's unit cell determine the diffracted beam's possible orientations. However, for powdered materials, crystallites are arranged randomly. The interaction of an X-ray beam with a powder occurs on all potential interatomic planes. By systematically altering the scanning angle of the detector, all potential diffraction peaks from the powder can be detected. Calculating the d-spacing from these diffraction peaks allows for material identification, as each substance has a distinct set of d-spacing values. This identification is accomplished by comparing the computed d-spacing with standard reference data. The XRD patterns of the samples were performed using SmartLab, a system from Rigaku Corporation, Japan, in the 2θ values spanning from 5° to 80°, utilizing Cu Kα radiation with a wavelength (λ value) of 1.5418 Å.

2.4.3 Thermogravimetric analysis (TGA)

TGA, a method widely employed for thermal analysis [32], measures the weight change relative to temperature or time. The experimental setup involves placing the sample in a temperature-programmed furnace. A sample pan with a precision balance is part of the TGA analyzer, and during the experiment, the pan undergoes heating or cooling in the furnace. A purge gas, which may be reactive or inert, regulates the sample environment. The heating is

programmable at a specific rate. Typically, the sample weight falls within the range of 1-10 mg, and in this instance, it was heated in a nitrogen atmosphere at a rate of 20 ºC/min, transitioning from 30 ºC to 800 ºC. An ultra-sensitive microbalance was used to track the weight fluctuations. Data on weight loss vs. temperature and time were captured online using the Shimadzu TGA-50 instrument from Japan.

Figure 2.4: Thermogravimetric analyzer (Shimadzu, TGA-50, Japan) used for the present work

2.4.4 Field emission scanning electron microscopy (FESEM) and energy-dispersive X-ray spectroscopy (EDX)

The topographical characteristics of the specimen were analyzed using FESEM. The FESEM allows for investigation of specimens with resolution down to the nm scale, achievable through a high-energy electron beam [33]. An electron microscope images a sample by scanning it with a high-energy electron beam. These electrons interact with the atoms of the sample, generating signals that offer insights into the sample's surface topography and composition. The signals produced by FESEM encompass secondary electrons, characteristic X-rays, backscattered electrons, cathodoluminescence, and transmitted electrons. By utilizing a secondary electron detector, FESEM can provide highly detailed images of a sample surface, revealing features as small as 1 to 5 nm. For effective FESEM imaging, the specimen must be electrically conductive, at least at the surface, to prevent the accumulation of electrostatic charge. Non-conductive specimens tend to charge during electron beam scanning, leading to scanning artifacts. To mitigate this, specimens are typically coated by conductive materials, like gold.

In present study, the morphology of the samples was performed using ZEISS SIGMA, FESEM system. This technique offers enhanced imaging capabilities compared to conventional

FESEM. ZEISS SIGMA employs a field emission gun that gives very narrow probing with both high and low energies, resulting in improved spatial resolution while minimizing sample damage and charging effects.

For the analysis of elemental sample chemical composition, EDX was employed. This technique is powerful for studying the elemental composition of samples, and elemental mapping provides insights into the distribution of materials in the matrix. When elements interact with X-rays, they eject core electrons, leaving behind a hole that can be filled by a high-energy electron, leading to the emission of unique energy signatures for every element in the periodic table. Further analysis was performed using the Bruker XFlash 6l100, which was attached to the FESEM instrument.

Figure 2.5: Field emission scanning electron microscopy (ZEISS SIGMA, Germany) and energy-dispersive X-ray spectroscopy (Bruker XFlash 6l100, Germany) used for the present work

2.4.5 Transmission electron microscopy (TEM)

Using highly accelerated electrons at high voltage in place of light, Transmission Electron Microscopy (TEM) uses the same optical principles as a light microscope [34]. Electrons, accelerated to high velocities, are utilized to illuminate an extremely thin specimen (200 nm), and as they traverse through, they scatter. This method offers the morphology of the sample at a resolution as fine as 1 nm or even smaller. Moreover, TEM produces an electron diffraction pattern, facilitating the revelation of molecular and atomic arrangements in crystalline specimens. The diffraction pattern in TEM arises from elastic scattering, providing insights into the local crystal structure.

In situations involving inelastic interaction between the primary electrons and electrons from the sample, particularly in the heterogeneities of nanostructures, complex absorption and scattering effects take place. This leads to spatial variations in the intensity of transmitted electrons, which can be detected by the detector during image formation.

For TEM imaging, the samples were dispersed in 2-propanol, and a droplet was deposited on the inner meshed area of a Copper (Cu) TEM grid with a diameter of 3 mm and a thickness and mesh size ranging from a few to 100 µm. Following that, the sample was vacuum-dried before imaging. TEM imaging was performed using a TEM-1400 PLUS instrument from JOEL India Pvt. Ltd., offering high-resolution capabilities.

Figure 2.6: Transmission electron microscopy (TEM-1400 PLUS, JOEL India pvt. Ltd.) used for the present work

2.4.6 Ultraviolet-visible spectroscopy (UV-vis)

UV-vis spectroscopy involves quantifying the reduction in intensity of a light beam in the visible, near UV, or IR range as it passes through or reflects from a sample surface [36]. During the traversal of light through the sample, electronic excitation occurs. The location of the absorption band corresponds to the wavelength of radiation whose energy matches the

requirement for the electronic transition from the ground state to the excited state. Absorption measurements can be performed at a single wavelength or across a wide spectral range. There exists a linear relationship between concentration and absorbance. Therefore, the concentration of an analyte in a solution can be ascertained by measuring the absorbance at a specific wavelength and applying the Beer-Lambert Law.

$$A = \varepsilon c l \quad (7)$$

Where A is an absorbance, ε is the absorptivity and c are the concentrations of the solution. The UV-vis absorption spectrum, based on this law, is a potent technique employed in the study of adsorption, particularly for pollutants in water, including the adsorption of colored materials such as dyes. The UV analysis in this work was performed on a Shimadzu 1800 instrument from Japan.

Figure 2.7: Ultraviolet-visible spectroscopy (Shimadzu 1800, Japan) used for the present work

2.4.7 Tensile properties

Tensile testing is a common method for determining tensile properties. This method commonly outlined by an American Society for Testing and Materials (ASTM) standard test [37]. In this procedure, a well-prepared test specimen is positioned between two jaws, typically one fixed and the other movable, within a universal testing machine (UTM). Force is applied to the specimen, generating a load vs. elongation curve. This curve is then transformed into a stress vs. strain curve, providing valuable information about the material's mechanical behavior under tension.

Tensile tests are employed to identifying various mechanical properties, including the elongation, tensile strength, modulus of elasticity, elastic limit, yield point, and yield strength, among others. In this specific investigation, tensile properties were performed using a Shimadzu universal testing machine with a crosshead speed of 50 mm/min, equipped with a load cell capacity

of 10 KN, and following the guidelines outlined in ASTM D 882. The initial length between the jaws at the commencement of every test was set to 50 mm. Each composite underwent testing with a minimum of five samples, and the average results were recorded. The Instron uniaxial test machine from the USA was employed for the analysis of tensile properties.

Figure 2.8: Tensile tester instrument (Instron uniaxial test machine, USA) used for the present work

2.4.8 Differential Scanning Calorimetry (DSC)

Differential Scanning Calorimetry (DSC) measures the heat flow difference between the reference material and the sample while both are subjected to a controlled temperature program [38]. It is a highly effective method for analyzing material characteristics like glass transition temperature, crystallization, melting, thermal stability, oxidation behavior, and specific heat capacity. DSC measurements of materials were performed using DSC-25, Shimadzu, Japan thermal analyzers. All sample was heated from 20 to 250 ºC at a rate of 5 ºC.min^{-1} under a N_2 atmosphere.

Figure 2.9: Differential Scanning Calorimetry (DSC-25, Shimadzu, Japan) used for the present work

2.4.9 Contact angle measurement

The contact angle measurement is a technique used to understand how a liquid interacts with a solid surface [39]. This measurement provides valuable information about the wetting properties of a material, helping to assess its hydrophobicity or hydrophilicity. The principle and working mechanism of contact angle measurement involve the assessment of the angle formed between the liquid droplet, solid surface, and the surrounding gas or vapor phase.

1.

Figure 2.10: Contact angle instrument (Krüss DSA100 contact angle goniometer, Germany) used for the present work

The contact angle formed at the intersection of these three phases reflects the balance of these intermolecular forces. A small contact angle indicates good wetting and strong attraction between the liquid and solid (hydrophilic), while a large contact angle indicates poor wetting and weaker interactions (hydrophobic). Contact angle measured using a Krüss DSA100 contact angle goniometer (Germany), utilizing deionized water at ambient temperature. To create a sessile drop on the PNC membrane films' surface, 5 mL of DI water was dispensed from a micro-syringe. For the analysis, an average of eight measurements was taken.

2.5 References

[1] Y. Zhu, S. Murali, W. Cai, X. Li, J. W. Suk, J. R. Potts, and R. S. Ruoff, Advanced Materials **22**, 3906 (2010).

[2] S. Stankovich, D. A. Dikin, R. D. Piner, K. A. Kohlhaas, A. Kleinhammes, Y. Jia, Y. Wu, S. T. Nguyen, and R. S. Ruoff, Carbon N Y **45**, 1558 (2007).

[3] S. He, X. Liu, P. Yan, A. Wang, J. Su, and X. Su, RSC Adv **9**, 4908 (2019).

[4] S. Singh, A. Bhadoria, K. Parikh, S. K. Yadav, S. Kumar, V. K. Aswal, and S. Kumar, J Phys Chem B **121**, 8756 (2017).

[5] D. Hirpara, B. Patel, V. Chavda, A. Desai, and S. Kumar, J Mol Liq **364**, 119991 (2022).

[6] W. S. Hummers and R. E. Offeman, J Am Chem Soc **80**, 1339 (1958).

[7] D. C. Marcano, D. V. Kosynkin, J. M. Berlin, A. Sinitskii, Z. Sun, A. Slesarev, L. B. Alemany, W. Lu, and J. M. Tour, ACS Nano **4**, 4806 (2010).

[8] W. Choi, I. Lahiri, R. Seelaboyina, and Y. S. Kang, Critical Reviews in Solid State and Materials Sciences **35**, 52 (2010).

[9] R. A. K. Rao, S. Singh, B. R. Singh, W. Khan, and A. H. Naqvi, J Environ Chem Eng **2**, 199 (2014).

[10] V. Chavda, B. Patel, S. Singh, D. Hirpara, V. D. Rajeswari, and S. Kumar, RSC Sustainability (2023).

[11] R. S. Das, S. K. Warkhade, A. Kumar, and A. V. Wankhade, Research on Chemical Intermediates **45**, 1689 (2019).

[12] R. Wang, K. Shi, D. Huang, J. Zhang, and S. An, Sci Rep **9**, 18744 (2019).

[13] E. D. H. Kong, J. H. F. Chau, C. W. Lai, C. S. Khe, G. Sharma, A. Kumar, S. Siengchin, and M. R. Sanjay, Nanomaterials **12**, 3536 (2022).

[14] R. Wang, K. Shi, D. Huang, J. Zhang, and S. An, Sci Rep **9**, 18744 (2019).

[15] J. T. Adeleke, T. Theivasanthi, M. Thiruppathi, M. Swaminathan, T. Akomolafe, and A. B. Alabi, Appl Surf Sci **455**, 195 (2018).

[16] T. Cun, C. Dong, and Q. Huang, Appl Surf Sci **384**, 73 (2016).

[17] S. Singh, B. Patel, K. Parikh, and S. Kumar, ChemistrySelect **5**, 14230 (2020).

[18] E. L. Smith, A. P. Abbott, and K. S. Ryder, Chem Rev **114**, 11060 (2014).

[19] M. S. Rahman and D. E. Raynie, J Mol Liq **324**, (2021).

[20] C. Bărdacă Urducea, A. C. Nechifor, I. A. Dimulescu, O. Oprea, G. Nechifor, E. E. Totu, I. Isildak, P. C. Albu, and S. G. Bungău, Nanomaterials **10**, 2349 (2020).

[21] V. Selen, Ö. Güler, D. Özer, and E. Evin, Desalination Water Treat **57**, 8826 (2016).

[22] M. Saxena, N. Sharma, and R. Saxena, Surfaces and Interfaces **21**, 100639 (2020).

[23] S. S. Tripathy and S. B. Kanungo, J Colloid Interface Sci **284**, 30 (2005).

[24] H. D. Patel and N. K. Acharya, Polym Eng Sci **61**, 2782 (2021).

[25] H. D. Patel and N. K. Acharya, Chem Eng Technol **45**, 2223 (2022).

[26] H. D. Patel and N. K. Acharya, Int J Hydrogen Energy (2023).

[27] M. W. J. Luiten-Olieman, L. Winnubst, A. Nijmeijer, M. Wessling, and N. E. Benes, J Memb Sci **370**, 124 (2011).

[28] A. K. Itta, H.-H. Tseng, and M.-Y. Wey, Int J Hydrogen Energy **35**, 1650 (2010).

[29] A. Dutta, in *Spectroscopic Methods for Nanomaterials Characterization* (Elsevier, 2017), pp. 73–93.

[30] A. A. Bunaciu, E. gabriela Udriştioiu, and H. Y. Aboul-Enein, Crit Rev Anal Chem **45**, 289 (2015).

[31] J. Kacher, C. Landon, B. L. Adams, and D. Fullwood, Ultramicroscopy **109**, 1148 (2009).

[32] P. Gabbott, editor , *Principles and Applications of Thermal Analysis* (Wiley, 2008).

[33] K. D. Vernon-Parry, III-Vs Review **13**, 40 (2000).

[34] R. C. Burghardt and R. Droleskey, Curr Protoc Microbiol **3**, (2006).

[35] Q. Lai, S. Zhu, X. Luo, M. Zou, and S. Huang, AIP Adv **2**, (2012).

[36] M. Basha, *Colorimetry and Spectrophotometer (Spectrophotometry)* (2020), pp. 23–38.

[37] H. Ku, H. Wang, N. Pattarachaiyakoop, and M. Trada, Compos B Eng **42**, 856 (2011).

[38] Y. Utievskyi, C. Neumann, J. Sindlinger, K. Schutjajew, M. Oschatz, A. Turchanin, N. Ueberschaar, and F. H. Schacher, Nanomaterials **13**, 2498 (2023).

[39] D. Y. Kwok and A. W. Neumann, Adv Colloid Interface Sci **81**, 167 (1999).